Atmospheric Environment Vol. 19, No. 12, pp. 2025–2031, 1985
Printed in Great Britain.

0004–6981/85 $3.00 + 0.00

AEROSOL MEASUREMENTS IN CENTRAL ALASKA, 1982–1984

GLENN E. SHAW
Geophysical Institute and Department of Space and Atmospheric Physics, University of Alaska, Fairbanks, Alaska 99701, U.S.A.

(*First received* 5 *November* 1984, *in final form* 28 *January* 1985 *and received for publication* 31 *May* 1985)

Abstract—Atmospheric aerosols in subarctic central Alaska were studied for two winter seasons. Both optical absorptivity and excess (non-marine) sulfate undergo seasonal variation similar to that reported in Arctic locations (maximum in late spring and minimum in summer), but the magnitudes are a factor of two smaller than in the Arctic. The meridional variation in aerosol blackness and sulfur content (cleaner air to the south) is contrary to the trend in the Scandinavian Arctic and is interpreted to indicate the existence of pollution sources generally north and west, outside of Alaska's borders.

Aerosol size varies with air temperature. Submicrometer aerosol mass and geometric mean diameter (GMD) increase as temperature decreases. Aerosols in all air masses studied were rich in volatile particles. The volatility suggests the presence of aqueous solutions of H_2SO_4. On the basis of (a) the relativity high aerosol volatility, and (b) the opposite trends between mean diameters and air temperature, it is conjectured that condensation of H_2SO_4 vapor may be an important mechanism for aerosol evolution in the winter (dark) polar troposphere.

Key word index: Arctic haze, graphitic carbon, sulfate, aerosol, atmospheric chemistry.

INTRODUCTION

Aerosol measurements were made in central Alaska during winter months at two isolated field sites: Ester Dome Observatory (64.9°N, 148°W, 715 m ASL) and Poker Flat Rocket range (65.1°N, 147.5°W, 375 m ASL). Both sites are on hills rising from floodplains between the Brooks Range to the north and the Alaska Range to the south. These sites were very clean and virtually free of contamination. The southern mountains act as barriers to the inflow of moist air from the Pacific Ocean and accordingly interior Alaska has a severe continental climate with an extreme range of seasonal temperature variation (annual mean temperature ~ -3°C, mean precipitation ~ 30 cm water equivalent). It is believed that aerosols measured at the sites in central Alaska during winter are representative of tropospheric aerosols in large, synoptic scale, air mass systems (see Bilello, 1974 for discussion of Alaskan air mass types).

Here we contrast the size distribution and chemistry of aerosols in two extreme air mass types: (a) air masses originating in the northern Pacific Ocean and (b) air masses originating from the Arctic Basin. The former systems tend to be moist and warm, while the latter are cold and dry and are sometimes charged with aerosol of anthropogenic origin (Raatz and Shaw, 1984; Hoff *et al.*, 1983).

SIZE CLASSIFYING THE AEROSOL

Tropospheric aerosol is distributed over a wide variety of particle sizes. Very little information is available on high latitude aerosol so we decided to size classify the aerosol over as wide a range as possible: this necessitated the use of a variety of methods. The experimental work was quite difficult because the Alaskan aerosol populates the region of the Greenfield (1957) 'gap' (~ 0.05–0.1 μm diameter) where no single aerosol sizing instrument works very satisfactorily. Table 1 summarizes the methods.

Table 1. Aerosol sizing experiments

Physical principal	Instrumentation	Diameter size range (μm)
Optical scattering	Laser spectrometer particle measuring system model LASX	0.15–3.0
Diffusive separation	Diffusion Screens	$\sim$ 0.005–0.1
Electrical mobility	Differential mobility particle sizer TSI Corp. Model 3071	0.01–0.3
Direct examination	Electron microscopy	0.05–10.0

Method 1

A commercial laser aerosol spectrometer (Particle Measuring Systems, Inc model LAS-X) classified 'large' and 'giant' particles by directing them in a focused stream through the central portion of a laser beam (TEM_{00} mode, λ = 632.8 nm) where they scatter a light pulse into a parabolic optical collecting system.

The system was calibrated with latex spheres and with monodisperse aerosol from an electrostatic classifier (TSI, Corp., model 3071). Figure 1 shows the calibration setup and some sample results.

Analysis of the sensitivity to index of refraction, n, for an instrument with similar light scattering geometry as the one used (ASASP-X) (Garvey and Pinnick, 1983) indicates that water droplets (n = 1.33) will be underestimated in size by ~ 10%, whereas crustal material (n = 1.55) will be overestimated by ~ 8%. The calibration curve adopted for the experiments assumed that n = 1.4, which would be appropriate for aqueous solutions of H_2SO_4 (Steele and Hamill, 1981). We will show experimental evidence later indicating that the predominant aerosol occurring in Alaska is H_2SO_4.

Method 2

The diffusion method is based on theory which treats an aerosol particle as a heavy molecule in kinetic equilibrium with its carrier gas (Einstein, 1956). Particles 'diffuse' under the driving action of thermal Brownian motion to the walls of microscopic pores where, upon contact, they adhere and are lost from the flow. The fraction of particles surviving passage through the diffusion screens is a function of

$$\psi = DN\ell/Q$$

where N is the number of microscopic pores, each of length ℓ, Q is volumetric flow rate and D is the diffusion coefficient for the particles. The product $N\ell$, the diffusion length of the battery, varied from 400 to 6×10^5 cm; Q was varied from 5 to 65 $cm^3\ s^{-1}$. The diffusion coefficient, D, is, in turn related to the particle diameter d, by the modified Stokes expression,

$$D = (kT/3\pi\eta d)\,(1 + AKn + BKn\exp(C/Kn))$$

where k is Boltzmann constant, T is temperature (°K), η is the carrier gas viscosity, Kn is the Knudsen number (ratio of molecular mean free path to particle diameter) and A, B and C have the numerical values 2.51, 0.88 and −0.435, respectively (Millikan, 1923).

Flow rates, Q, through the filters were chosen to provide filter functions with 50% cut off points equally spaced in log diameter from 0.005 to 0.1 μm (Fig. 2). Twelve filter-flow combinations were used initially, but in later experiments this was reduced to eight (Fig. 2) (Gras, 1983).

Particles surviving passage through the screens were counted with a continuous flow Condensation Nucleus Counter (CNC) (TSI, Inc., model 3020) using butanol as the working fluid (Agarwal and Sem, 1980). The lower limit of size detected with such a CNC counter is ~ 0.005 μm. After filtering, the count was sometimes very low (e.g. 0.05 cm^{-3}).

The aerosol size spectra were calculated with the non-linear inversion algorithm (Twomey, 1975). After 100 iterations the residuals were typically in the range 5–10%; since the measurements were of about this level of precision no further improvement would result by performing more iterations.

The method of Park *et al.* (1980) was also used to derive equivalent log-normal distribution fits of the aerosol size distributions at submicrometer sizes.

Method 3

In spring 1984, sizing by electric mobility separation was added to the suite of aerosol sizing experiments to gain additional information about the number size spectrum in the (difficult) diameter range 0.01–0.1 μm. Air containing particles is drawn through a Kr85 ionization source ($Nt = 10^7$ ion pairs cm^{-3} s) to bring the aerosols into charge equilibrium (which is assumed in the data analysis to be the Boltzmann distribution) and then enters an electrostatic classifier (TSI Corp., model 3071) to select particles in a

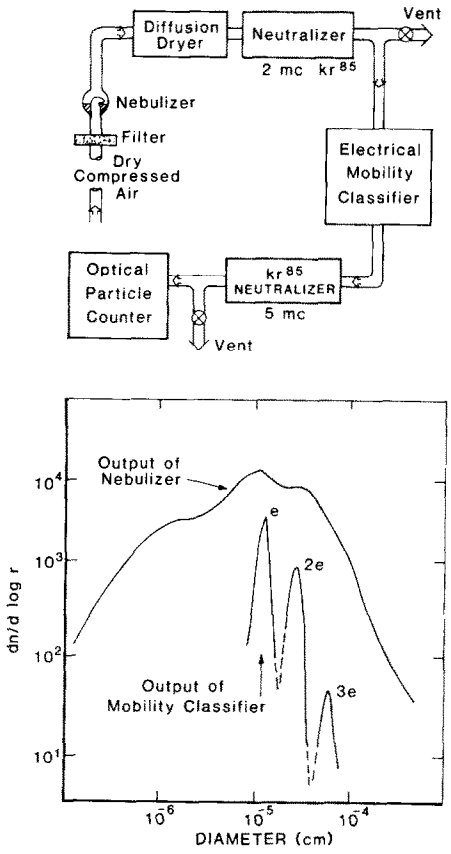

Fig. 1. (a) Setup used to calibrate the optical particle counter. Particles exiting the mobility classifier are nearly monodisperse (geometric standard deviation, $\sigma_g \sim 1.1$). (b) Example results of the calibration: multiple peaks are due to particles with n = 1.2, 3 . . . , elementary charges with 1/2, 1/3 . . . , mechanical mobility of single charged particles.

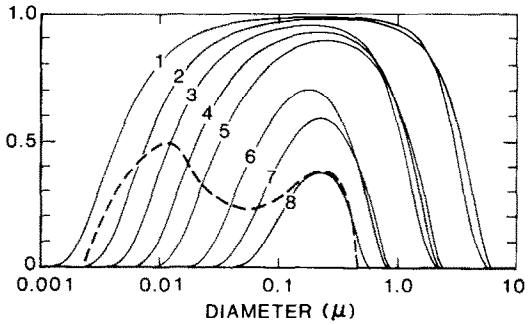

Fig. 2. Transmission characteristics of the diffusion screens. The eight filter-flow curves are combinations of Nuclepore filters with nominal pore diameters ranging from 0.6 to 8 μm and face velocities ranging from 1.4 to 8.8 cm s^{-1}. The theory of Manton (1978) is used to calculate the functions. The dotted line represents a typical bimodal aerosol size distribution spectrum.

range of electrical mobility $dB/B \sim 0.1$. The monodisperse particles which exit are counted with the TSI model 3020 continuous flow CNC counter. An inertial impactor is placed in the inlet line to remove particles larger than $\sim 0.2\ \mu m$ in order to prevent possible ambiguities which may otherwise arise (singly charged particles have identical electrical mobility to doubly-charged particles with half the mechanical mobility). Recovery of the size spectrum is based on the method of Hoppel (1978).

CHEMICAL MEASUREMENTS

Mass concentrations of anions (SO_4^{2-}, NO_3^-, Cl^-) collected on 3.5-cm diameter filters were determined by ion chromatography (Dionex model 20). Typical blank levels for SO_4^{2-} were only a few percent of aerosol sulfate, but nitrate and phosphate concentration on blanks were relatively more significant and variable, making the determination of those species less reliable. Precision is estimated at $\sim 10\%$ for sulfate and 50% for nitrate and phosphate. Most filters were exposed for a week at Poker Flat.

The optical absorption coefficient of the aerosol, β_a, (m^{-1}) was estimated with the Integrating Sandwich technique (Clarke, 1982) using illumination from a monochromator (λ = 500 nm) and a photoelectric detecting system. The experimental technique was calibrated by (1) referencing to the (less sensitive) integrating plate method (Lin *et al.*, 1973) and (2) gravimetric determinations of soot with known specific absorbance (Stevens *et al.*, 1982). Precision of the method is estimated to be $\pm 5 \times 10^{-8}\ m^{-1}$ and accuracy $\pm 1 \times 10^{-7}\ m^{-1}$; typical coefficients were $5\text{–}10 \times 10^{-7}\ m^{-1}$ in winter.

THE SITES

Poker Flat Research Range (PFRR), 75 km north of Fairbanks, is isolated meteorologically from Fairbanks by intervening hills. The site has no direct combustion sources (electric heating is used) and experiences very little traffic. Aerosols were collected from the optical observatory site 215 m above the rocket range. Aitken nuclei concentrations at the optical observatory are normally one to a few hundred cm^{-3} during the winter months.

Precipitation at PFRR averages 28 cm water y^{-1}, about two thirds of which falls in the summer months. The chemistry of precipitation at the site is as follows (Galloway *et al.*, 1982): mean pH = 4.96; dominant cations are 10.5 $\mu eq\ \ell^{-1}$ SO_4^{2-} and 2.4 $\mu eq\ \ell^{-1}$ NO_3^-. Arithmetic mean hydrogen ion concentration at PFRR is 11.8 $\mu eq\ \ell^{-1}$.

Ester Dome Observatory (EDO) is on a 'dome' rising ~ 580 m above the floodplain of the Tanana River 20 km west of Fairbanks. The site experiences occasional contamination from houses on the slope of the dome when winds are in the segment 100–140°. The site is equipped with meteorological instrumentation.

RESULTS

Larger aerosol: relation to air mass type

Figure 3 refers to the aerosol number concentrations in a narrow size interval centered at 0.3 μm; this size interval was chosen because it lies near the maximum of the aerosol mass spectrum and therefore is indicative of submicrometer aerosol mass loading. Shown above the submicrometer aerosol concentration is a time–height plot of potential temperature which is useful in identification of different air mass incursions into interior Alaska.

Intrusions of warm air into central Alaska are associated with lower than usual aerosol volume, whereas intrusions of cold, Arctic-derived, air masses tend to be associated with higher than normal aerosol volume. As explained later this does not necessarily mean that Arctic air is more polluted.

It should be noted that the aerosol plotted in Fig. 3 is of a size near the 'Greenfield Gap' where the predominant mass of particulate material is generally highest in well-aged air mass systems: this component is referred to from now on as the 'accumulation mode'.

The systematic relation between aerosol 'accumulation mode' concentration and air mass origin, suggested by Fig. 3 is corroborated in plots of aerosol concentration and daily mean air temperature. For example, the scatter diagram of the daily mean temperature against aerosol number concentration is illustrated in Fig. 4a for particles in the accumulation

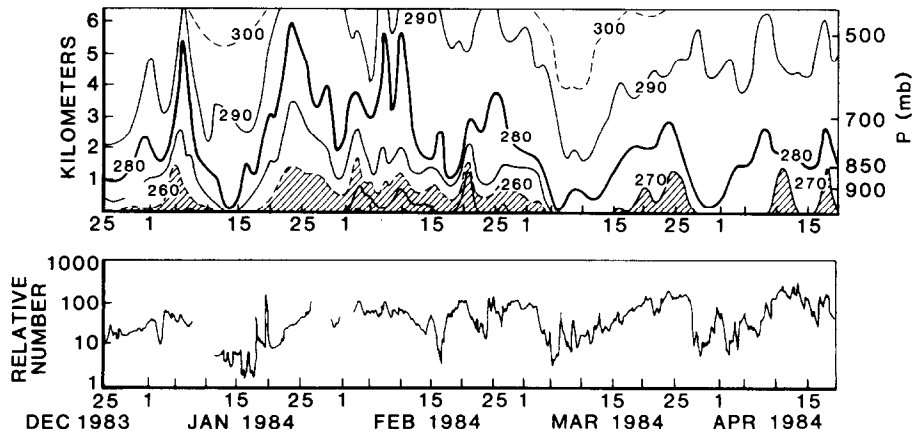

Fig. 3. (a) Height-time cross-section of potential temperatures for late winter, spring, 1984 for central Alaska. Pacific Marine air mass intrusions occur in dips, while intrusions of Arctic-derived air masses are represented as peaks. (b) 4 h averages of aerosol number concentration at EDO in a narrow size bin located near the centroid of the accumulation model ($\bar{d} = 0.3\ \mu m$).

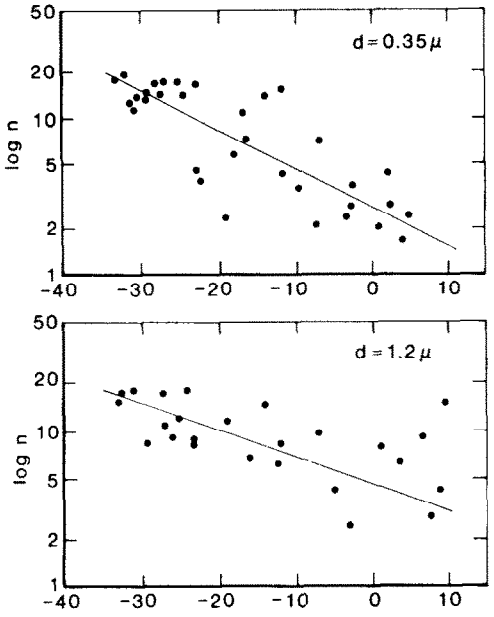

Fig. 4. Scatter diagram showing the correlation between air temperature (abscissa) and number particle concentration in narrow size bins at (a) 0.35 μm, (b) 1.2 μm.

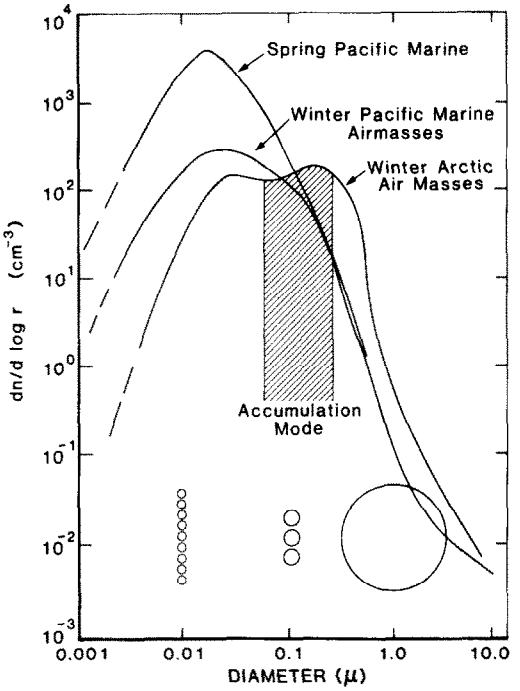

Fig. 5. Characteristic aerosol number size distributions (number cm^{-3} per decade of diameter) for (a) winter Arctic-derived air masses, (b) winter Pacific–Marine systems and (c) Pacific systems around vernal equinox when solar radiation becomes significant following the semi-polar night.

mode ($\bar{d} = 0.35\ \mu$) and for larger sized particles ($d = 1.2\ \mu$) in Fig. 4b.

Aitken aerosol

The geometric mean particle number concentration at Ester Dome was 350 cm^{-3} (December 1983–March, 1984, excluding data from the contaminated sector from 100 to 140°); the distribution of number counts was approximately log normal with geometric standard deviation, $\sigma_g = 2.4$. Quartile values of n were $n_1 = 190\ cm^{-3}$ and $n_3 = 650\ cm^{-3}$. The lowest concentration observed ($\sim 70\ cm^{-3}$) occurred in persistent anticyclonic systems and during the months December and January when sunlight illumination was insignificant.

During the cold, dark months in central Alaska the particle number concentration would sometimes remain nearly constant, varying by no more than $\sim 10\%$ over hours and sometimes even days of time. Typically, during these very stable episodes the wind was steady from the north to northwest, it was cold (−20 to −30°C), sunlight was negligible and back trajectories at the 850 mb level led to central Eurasia or (less frequently) to regions in northern Canada. Incoming Pacific Marine air masses had slightly higher (e.g. 50%) number concentration, but tended to vary over shorter time scales than the cold intrusions.

Aerosol size

Aerosol size distributions fell into three categories illustrated in Fig. 5: (a) those which occurred during excursions of well defined, cold, dry 'Arctic' air masses, (b) those which occurred during sustained 'warm' air flows from the northern Pacific Ocean (Pacific Marine air mass types), and (c) those which occurred around the time of vernal equinox when significant solar radiation fluxes occur for the first time following the semi-polar night. Aerosol distributions later in the spring, after the time of snow melt and following spring vegetational growth, is complex and variable and is not treated in this paper.

Note that during the dark months there are substantial differences in the size spectrum of the tropospheric aerosol during intrusions of warm Pacific Marine and cold 'Arctic' air mass systems, the mean size being about half an order of magnitude smaller for the warm Pacific Marine air masses. At the same time, the number concentration of aerosols (as measured with CCN counters and incorporating all particles larger than about 0.005 μm) is comparable for the two widely differing air mass types. Arctic air masses contain, then, an order of magnitude greater mass loading than the warm intrusions of air from the Pacific Ocean region. These differences in size and mass of the aerosol in the two greatly different air masses is a repeatable and general feature which to our knowledge has not been reported before.

Sulfate and aerosol blackness

Excess (non-marine) sulfate, SO_4, ($\mu g\ m^{-3}$) and aerosol optical extinction coefficient β_a (m^{-1}) undergo seasonal variation (Fig. 6) similar to that observed at

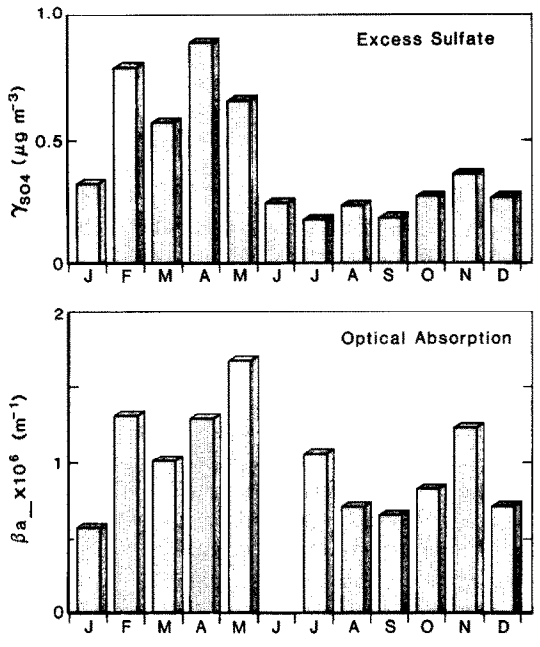

Fig. 6. Monthly mean values of excess sulfate (a), and aerosol optical absorption coefficient (b), in central Alaska. Years 1981–1984.

other Arctic locations (Barrie *et al.*, 1981; Joranger and Ottar, 1984; Rahn and Shaw, 1982) with maxima in late winter–early spring and minima in summer.

The optical absorption coefficient (500 nm wavelength), β_a, and 'excess' sulfate correlate as follows for different seasons:

$$\text{I } SO_4 = 0.33 + 0.025 \times 10^{-7}\,\beta_a \quad \text{(January–May)}$$

$$\text{II } SO_4 = 0.26 + 0.007 \times 10^{-7}\,\beta_a \quad \text{(July–September)}$$

$$\text{III } SO_4 = 0.10 + 0.021 \times 10^{-7}\,\beta_a \quad \text{(October–December)}$$

where SO_4 is in units of $\mu g\ m^{-3}$ and β_a in units m^{-1}.

The seasonal categories above were chosen as follows: I represents the period of maximum air pollution which is from Arctic sources, II represents the period of minimum air pollution when cloud occurrence and scavenging is high and precipitation is maximum, III represents the period of transition between the 'polluted' late winter–spring and 'unpolluted' summer.

It is obvious from the color of the filters that summer collections are contaminated with blowing crustal material (loess): the filters are brown, whereas filters exposed during the snow-covered months are uniformly gray and presumably affected mainly by graphitic carbon (Rosen *et al.*, 1981). The tan-brown color of summer filters in fact is identical to the color of the soil material around the sampling location. If soil contamination is responsible for the absorption in summer, as we hypothesize, one would expect higher than normal ratios of β_a/SO_4 than during snow-covered months. $\beta_a/SO_4 = 385$ (period II), β_a/SO_4^{2-} 19 (period I), β_a/SO_4^{2-} 30 (period III). The hypothesis of significant amounts of local crustal contamination for summer β is confirmed.

In all three seasonal cases, when $\beta_a \to 0$, a residual from 0.1 to 0.3 $\mu g\ m^{-3}$ of SO_4 remains. This may represent a naturally-occurring background sulfate since the concentrations are similar to these reported in Antarctica (Maenhaut *et al.*, 1979).

Arithmetic mean values of SO_4 and β_a for the three periods are in Table 2.

Aerosol volatility

The molecular form of the aerosol is unknown, but some insight has been obtained from experiments on the evaporation of aerosol at elevated temperature fields (for the technique see Dinger *et al.*, 1970). Air was pulled through an electrically heated fused silica tube furnace (5 mm diameter, 40 cm in length) at a (laminar) flow rate of 5 $cm^3\ s^{-1}$. Particle concentration in the narrow size bin ~ 0.2 μm diameter was monitored before heating and after heating (to a temperature of ~ 150°C) and typically we found that the concentration would drop by about an order of magnitude. Thus most accumulation mode aerosols were fairly volatile, H_2SO_4 aqueous droplets decompose at the temperature used, but NaCl or crustal material does not.

The fraction, f, of particles with mean diameter 0.2 μm surviving passage through the temperature field varied. Based on experiments performed approximately every other day from January to April 1984, it ranged from 0.18 to 0.06 with a geometric mean of 0.085. Therefore $\sim 85\%$ of the aerosol was volatile enough to evaporate in less than the time required to transit the heated tube.

Attempts to relate the variability of f to large air mass features have so far been unsuccessful. We can find no significant correlation with temperature, air mass, aerosol number, mass loading, etc., though there is a weak correlation ($c = 0.3$) between f and wind direction, the more non-volatile fraction being associated with winds from the S to SE sectors possibly contaminated by habitations nearby.

Table 2. Arithmetic means of sulfate and optical absorption coefficient β_a

Period	Season	SO_4 ($\mu g\ m^{-3}$)	β_a (m^{-1})
I	Late winter/spring	0.63	12.0×10^{-7}
II	Summer	0.24	$8.1^* \times 10^{-7}$
III	Autumn 'transitional'	0.29	9.2×10^{-7}
	Annual average	0.38	9.8×10^{-7}

*Crustal contamination.

DISCUSSION

Evidence of pollution sources north of Alaska

Seasonal mean excess sulfate mass was 0.38 $\mu g\ m^{-3}$ during 1984 in central Alaska, this is 1.7 times less than measured at Barrow, Alaska during the period October 1976–June 1978 (Rahn and Shaw, 1982). The ratio of arithmetic means of excess sulfate at Barrow to that in central Alaska is larger than unity for all seasonal categories (Table 3).

The larger sulfate mass in northern Alaska compared to that in central Alaska suggests pollution sources generally to the north (or NW) of Alaska. An opposite meridional gradient is found in the Scandinavian Arctic. Mass loading of SO_4^{2-} in Spitsbergen is about half the value in central Sweden. The latter is obviously nearer to significant industrial sources of sulfur-emitting pollution.

Speculations on the temperature-dependence of aerosol size

The increase in accumulation mode aerosol with decreasing air temperatures is a phenomenon (Figs 3 and 4) indicating quite clearly the existence of elevated aerosol mass in cold, Arctic-derived air. However, it does not necessarily follow from this that the increased aerosol mass loading is pollution-derived: it could in fact be largely derived from naturally occurring processes. The ratio of 'pollution' to 'natural' aerosol is at this stage an entirely open question. The question is all the more uncertain because of the size range in which the majority of the aerosol mass is found. The mass is in the range 10^{-5}–10^{-4} cm (i.e. the Greenfield Gap) where theory predicts it to be for a well-aged aerosol. If the aerosol is well aged, as its size would suggest, and as cold air flowing down into Alaska from the north also would suggest it to be, then natural processes (as opposed to anthropogenic pollution) occurring at slow rates and which may otherwise be rather unimportant, may become dominant in the creation and growth of aerosols. Such a process is the condensation onto pre-existing aerosol of a supersaturated vapor with a low saturation vapor pressure like H_2SO_4. The rate of impingement of H_2SO_4 molecules in the vapor state at several hundred percent supersaturation on a 10^{-6}-cm diameter particle is such that the growth rate to the accumulation mode (i.e. $\sim 10^{-5}$ cm) is on the order of time taken for air masses charged with pollutants in Eurasia to travel to Alaska. Thus, although one indeed finds evidence of pollution-derived metal residues (i.e. Raatz and Shaw, 1984) in Arctic air, one also finds 'too much sulfate' (Rahn, 1981). Our studies indicate a high proportion of sulfate particles and, for the reason stated, this sulfate can be conjectured to have arisen, possibly, by slow condensation of H_2SO_4 vapor which in turn has an uncertain origin: we cannot at this stage sort out the anthropogenic from the marine, biogenic oxidized sulfur products. The key point is that the long residence time of the Arctic aerosol favors the occurrence of slow growth processes like the condensation of vapor state H_2SO_4 molecules.

Table 3. Ratio of excess sulfate at Barrow to excess sulfate in central Alaska

I	Late winter–early spring	2.03
II	Summer	1.27
III	Autumn–early winter	1.51
	Seasonal average	1.68

On the adoption of the above viewpoint, the systematic inverse relationship between temperature (low temperatures are associated with well-aged Arctic air) and particle size is to be expected. Additionally, insoluble particles would be coated with a film of sulfuric acid which, by Rault's Law, would reduce equilibrium saturation vapor pressure making nonsoluble primary pollution particles potentially active at fairly low supersaturations as cloud condensation nuclei.

Acknowledgements—This work was supported by a grant from the National Science Foundation (grant No. ATM 8300155) and by State of Alaska funds.

REFERENCES

Agarwal J. K. and Sem G. J. (1980) Continuous flow, single-particle-counting Condensation Nucleus Counter. *J. Aerosol Sci.* **11**, 343–357.

Barrie L. A., Hoff R. M. and Daggupaty S. M. (1981) The influence of midlatitudinal pollution sources on haze in the Canadian Arctic. *Atmospheric Environment* **15**, 1407–1419.

Bilello M. A. (1974) Air masses, fronts and winter precipitation in central Alaska, CRREL Research Report RR319, Cold Regions Research and Engineering Laboratory, Hanover, New Hampshire.

Clarke A. D. (1982) Integrating sandwich: a new method of measurement of the light absorption coefficient for atmospheric particles. *Appl. Opt.* **21**, 301–319.

Dinger J. E., Howell H. B. and Wojcieokowski T. A. (1970) On the source and composition of cloud nuclei in a subsident air mass over the North Atlantic. *J. atmos. Sci.* **27**, 791–797.

Einstein A. (1956) Investigations on the theory of the Brownian movement, English translation of original 1905 paper by F. Furth (Ed), Dover Publications, New York.

Galloway J. N., Likens G. E., Keene W. C. and Miller J. M. (1982) The composition of precipitation in remote areas of the world. *J. geophys. Res.* **87**, 8771–8786.

Garvey D. M. and Pinnick R. G. (1983) Response characteristics of the particle measuring systems active scattering aerosol spectrometer probe (ASASP-X). *Aerosol Sci. Technol.* **2**, 477–488.

Gras J. L. (1983) An investigation of a non-linear iterative procedure for inversion of particle size distributions. *Atmospheric Environment* **17**, 883–894.

Greenfield S. M. (1957) Rain scavenging of radioactive particulate matter from the atmosphere. *J. Met.* **14**, 115–125.

Hoff R. N., Leaitch W. R., Fellin D. and Barrie L. A. (1983) Mass size distributions of chemical constituents of the winter arctic aerosol. *J. geophys. Res.* **88**, 10,947–956.

Hoppel W. A. (1978) Determination of the aerosol size distribution from the mobility distribution of the charged fraction of aerosols. *J. Aerosol Sci.* **9**, 41–54.

Joranger E. and Ottar B. (1984) Air pollution studies in the Norwegian Arctic. *Geophys. Res. Lett.* **11**, 365–368.

Lin C. I., Baker M. and Charlson R. J. (1973) Absorption coefficient of atmospheric aerosol: a method of measurement. *Appl. Optics* **12**, 1356–1363.

Maenhaut W., Zoller W. H., Duce R. A. and Hoffman G. L. (1979) Concentration and size distribution of particulate trace elements in the south polar atmosphere. *J. geophys. Res.* **84**, 2421–2431.

Manton M. J. (1978) The impaction of aerosols on a Nuclepore filter. *Atmospheric Environment* **12**, 1669–1675.

Millikan R. A. (1923) Coefficients of slip in gases and the law of reflection of molecules from the surfaces of solids and liquids. *Phys. Rev.* **21**, 217–238.

Park Y. O., King W. E., Jr. and Gentry J. W. (1980) On the inversion of penetration measurements to determine aerosol product size distributions. *Ind. Engng Chem. Prod. Res. Dev.* **19**, 151–157.

Raatz W. E. and Shaw G. E. (1984) Long-range tropospheric transport of pollution aerosols into the Alaskan arctic. *J. Clim. appl. Met.* **23**, 1052–1064.

Rahn K. A. (1981) Relative importance of North America and Eurasia as sources of Arctic aerosol. *Atmospheric Environment* **15**, 1447–1455.

Rahn K. A. and Shaw G. E. (1982) Sources and trasnport of arctic pollution aerosol: a chronical of six years of ONR research. *Naval Res. Rev.* **34**, 3–26.

Rosen H., Novakov T. and Bodhaine B. A. (1981) Soot in the Arctic. *Atmospheric Environment* **15**, 1353–1364.

Steele H. M. and Hamill P. (1981) Effects of temperature and humidity on the growth and optical properties of sulphuric acid–water droplets in the stratosphere. *J. Aerosol Sci.* **12**, 517–518.

Twomey S. (1975) Comparison of constrained linear inversion and an iterative non-linear algorithm applied to the indirect estimation of particle size distributions. *J. comp. Phys.* **18**, 188–200.